Mon. Not. R. astr. Soc. (1988) **231,** 1091–1115

Collisional properties of ice spheres at low impact velocities

Artie P. Hatzes *Lick Observatory, Board of Studies in Astronomy and Astrophysics, University of California, Santa Cruz, CA 95064, USA*

Frank G. Bridges *Board of Studies in Physics, University of California, Santa Cruz, CA 95064, USA*

D. N. C. Lin *Lick Observatory, Board of Studies in Astronomy and Astrophysics, University of California, Santa Cruz, CA 95064, USA*

Accepted 1987 October 30. Received 1987 October 30; in original form 1987 August 11

Summary. In this paper we discuss the results of our experimental studies on the impact properties of water ice. The measurements were made using a new apparatus consisting of a compound disc pendulum and a stainless steel, temperature controlled cryostat. With this apparatus we have been able to achieve stable temperatures of 85 K and pressures as low as 10^{-5} torr. Using a capacitive displacement device for accurately measuring the position of the pendulum during each collision, we have been able to obtain accurate measurements of the coefficient of restitution for ice spheres impacting with velocities in the range 0.015–2 cm s^{-1}. The coefficient of restitution as a function of velocity, $\varepsilon(v)$, for ice spheres with four different radii of curvature and with a variety of surface conditions has been obtained. The coefficient of restitution data can be well fitted by an exponential law of the form $\varepsilon(v)=C\exp(-\gamma v)$, for most measurements. We find, however, that the surface conditions can drastically alter the resulting value of ε. In particular the presence of frost or a roughened contact surface can lower ε at a given velocity by 10–30 per cent from that of a smooth sphere. We also show how the presence of frost can change the velocity behaviour of ε from an exponential to a power-law form. We briefly discuss the applications of our results to the dynamics of Saturn's rings.

1 Introduction

The global properties of planetary rings are basically determined by the collisional properties of the ring particles. In the case of the Saturnian ring system, water ice is the principal constituent (see review by Goldreich & Tremaine 1982). For example, the dynamical evolution of the rings is regulated by the collisionally induced viscous stress which is determined by the velocity dispersion of the particles (Goldreich & Tremaine 1978; Stewart, Lin & Bodenheimer 1984). Particle

collisions in a differentially rotating disc, such as planetary rings, induce the growth of the velocity dispersion. If these collisions are partially inelastic, their associated energy loss would cause the dispersive motion to be dissipated. In an energy equilibrium, a velocity dispersion is established such that these two processes are balanced. In order to evaluate the value of the velocity dispersion for a given surface density, we need some information on the energy lost during each collision which may be expressed in terms of the coefficient of restitution, ε.

In a previous paper, we described an experiment for measuring the coefficient of restitution as a function of impact velocity, $\varepsilon(v)$ (Bridges, Hatzes & Lin 1984, hereafter Paper I). In that preliminary report, we used ice particles with a radius of 2.75 cm and an uncontrolled surface crystal structure to perform experiments at $T\sim170$ K and at atmospheric pressure. Despite the relatively simple experimental set up, we established $\varepsilon(v)=0.32v^{-0.24}$ for $v>0.05$ cm s^{-1}. Applying this to Saturn's rings, we estimated the thickness of the ring to be less than 5 m.

Although this early experiment led to useful information, additional data were needed. For example, the ring particles have a size distribution over several orders of magnitude (Cuzzi *et al.* 1984) so that data on the size dependence of ε would be desirable. The size dependence in $\varepsilon(v)$ may induce different size particles to establish a range of equilibrium conditions. A size dependence in the equilibrium velocity dispersion could lead to particle-size segregation in the direction normal to the plane as well as in the radial direction of the rings. Such a model may be applied to *Voyager's* data to provide a dynamical explanation for the observed difference in the surface-density variation, along the radial direction, among particles with different sizes (Marouf *et al.* 1983). It is also of interest to evaluate the dependence of ε on the surface crystal structure of the ice particles. Since the surface structure may be modified by the ambient environment, it is important to carry out the experiment in a cryostat where the temperature and pressure can be closely controlled. Finally, in some regions such as the B ring, the velocity dispersion of the particles may be somewhat smaller than the previously measured cases. Data on low-velocity impacts may also be useful. In this paper, we present our new data on ice particle collisions. We describe our modified apparatus in Section 2 and outline our results in Section 3. Finally, in Section 4, we discuss the implication of these results on the structure and evolution of Saturn's rings.

2 The apparatus and experimental methods

In order to achieve the above objectives, it was necessary to upgrade our previous apparatus in four areas: (i) a new cryostat capable of achieving lower temperatures with good temperature stability, (ii) a measurement device to accurately determine the ice particle's position before, during, and after each impact, (iii) complete computer control of the data acquisition and analysis and (iv) a more closely controlled sample preparation procedure.

The heart of the apparatus is essentially the same as the previous experiment, namely a compound disc pendulum constructed from aluminium. The salient features of this device are shown in Fig. 1 which is a schematic viewed along the rotation axis. If the centre of mass of the disc lies at a distance h below the pivot point then the angular frequency of oscillation of the system is given by $(mgh/I)^{1/2}$, where I is the moment of inertia, m the mass of the system, and g is the acceleration of gravity. By adjusting the centre-of-mass of the system we can obtain arbitrarily long periods of oscillation for the system. Typically we run at periods of 10–40 s. The current disc pendulum (with ice sphere) has a moment of inertia of about 10^5 g cm^2 compared to 1.4×10^5 g cm^2 for the previous one. Since the collisions are not free, this moment of inertia has the effect of increasing the effective mass of the ice spheres to 450 g from the 60 g for a freely moving 2.5-cm radius ice sphere (450 g is near the mass expected from a 5-cm radius ice sphere). Thus at a given velocity, our ice spheres have greater energy than freely colliding particles of 2.5-cm radius; when

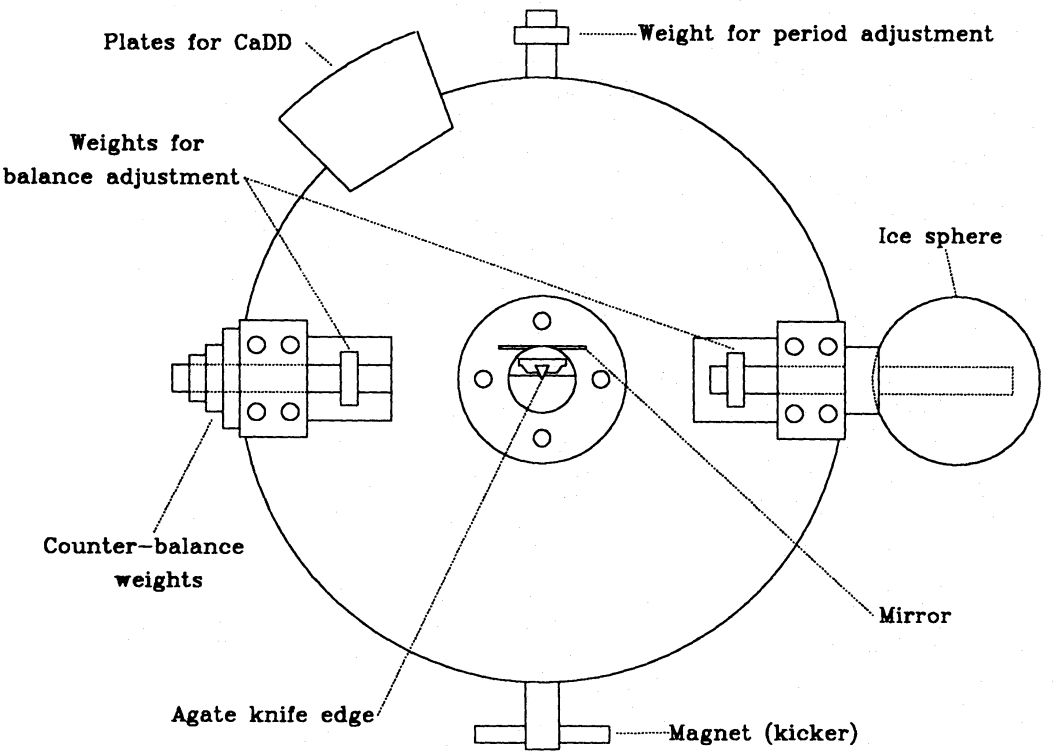

Figure 1. Front view of the disc pendulum showing the important features. The radius of the ice sphere shown is 2.5 cm.

a larger radius of curvature (10 or 20 cm) is moulded onto the ice sphere, we are in the opposite limit, and the energy is less than that for the freely colliding particles of equivalent radius.

As indicated in Fig. 1, ice balls are mounted on one side of the pendulum and counter-balance weights on a threaded rod are located on the opposite side. Adjustment weights on this rod enable us to balance the pendulum so that the ice sphere-counterweight axis is horizontal. An additional adjustment weight on another short threaded rod occupies a position on the top of the pendulum. This weight is used for adjusting the period of oscillation of the system by changing the location of the centre of mass with respect to the disc axis. The pivot points of the pendulum consist of agate knife edges that rest on polished agate blocks. The flexure of these blades during oscillation of the pendulum is small and thus they are excellent for keeping friction in the system to a minimum. A typical damping constant, γ [where we have defined the damping of the amplitude of the oscillation as a function of time, t, as $\exp(-\gamma t)$] is 0.01 s^{-1}. This term has a negligible effect on the velocity over the time period of the measurements (typically 0.05–0.1 s).

The fact that the collisions are not free is a source of concern since the coupling of the ice sphere to the pendulum causes a slight elastic deformation of the pendulum during the collision, resulting in additional energy losses as vibrations and some stored elastic energy that can be reconverted to mechanical motion. Efforts were made to minimize such flexures. The thickness of the new disc was increased by 50 per cent (from 3.2 to 4.8 mm) over the previously used disc. Also the ice sphere and all counterweights were placed close to the disc so as to minimize torques. A special design was also made for the mount which couples the ice sphere to the disc, structurally the weakest part of the pendulum system. Referring to Fig. 1, this mount consists of a single machined aluminium rod with a 2.5-cm diameter support section at the centre of the rod. This central portion of the rod is pressed firmly against a square mount on the pendulum disc. One side of the central piece is concave with a radius of curvature the same as the ice spheres. This provides

a contoured surface which fits snugly about the ice sphere. As a test we also made several runs replacing the aluminium mount with a steel rod 1 cm in diameter. The resulting data were identical to that taken using the aluminium mount. This would not have been the case if energy losses or stored energy due to flexures of the ice mount were important since different materials would yield different amounts of energy loss or transfer. For a few cases, with an extremely smooth ice surface, the measured ε is greater than 0.8 for $v=2\,\mathrm{cm\ s^{-1}}$. We conclude that the coefficient of restitution that we measure is primarily due to energy losses of the ice sphere at the contact surface rather than deformations of the pendulum system.

The new cryostat, a stainless steel double walled chamber, provides a stable low-temperature and low-pressure ambient environment. The pressure in the air space between the two walls of the chamber can be varied to control the thermal conduction from the outer walls of the chamber (usually at 80 K) and the inner chamber. The pendulum is mounted at the bottom of this cryostat within a cylindrical copper can. A 4.5-cm-thick plate of acrylic serves the dual purpose of lid and window to this cryostat. This acrylic window also has a glove box which provides access to the pendulum for making final adjustments on the balance or to ensure that it is seated properly on the agate blocks, even at low temperatures. The advantage of this new cryostat is that the fine adjustments of the pendulum (which are usually the most time consuming) can now be made with the pendulum and ice sphere in a cold, nitrogen-rich atmosphere.

We have dramatically improved the method of measuring the velocity of the ice spheres prior to and after each collision as well. This was accomplished by the construction of a capacitive displacement device (CaDD) which uses the varying capacitance of a system of plates for measuring the displacement of the pendulum. The operation of this device is shown in Fig. 2. The CaDD consists of two sets of parallel plates. One set of six blades is mounted on the pendulum as indicated in Fig. 1. A complementary set of eight blades is mounted to the side of the inner copper can; when in place these blades are configured such that a pendulum blade rests between two fixed blades. As the pendulum oscillates the blades on the pendulum freely move between the stationary ones mounted on the copper can which actually consists of three separate sets of blades (labelled A, B and C in Fig. 2). An oscillating square wave voltage is applied to set A while an identical voltage, 180° out of phase, is applied to set C. The central segments B act as a receiver. The amount of signal the central segments receive from the outer two segments depends on the common area between those segments and the blades mounted on the pendulum. Near the equilibrium position of the pendulum the overlapping area of the disc blades with set A equals the overlapping area with set C. This results in an output voltage of 0 (top panel of Fig. 2). If the pendulum is now displaced to one side, the overlapping area of the disc blades and blades A is now greater than that for set C. The receiver thus detects more of the signal on A than C and this results in a positive voltage $+V_0$ from the CaDD (central panel). If the pendulum is displaced by an equal amount to the other side, then the signal from the B segments dominates resulting in a negative voltage $-V_0$ (last panel). The net result is that the CaDD produces a voltage which is directly proportional to the displacement of the pendulum. The output voltage is calibrated against known displacements of the pendulum which are obtained using the displacement of a laser beam reflected from a mirror mounted on the pendulum axis of rotation. Fig. 3 shows a typical calibration of voltage from the CaDD as a function of displacement of the pendulum. This device is quite linear and stable. The calibration, which is made before and after each experimental run, changes by no more than 0.5 per cent during the course of an experimental run and by no more than 1–2 per cent from run to run.

The output of the CaDD is interfaced to a microcomputer via a medium speed analog to digital converter (ADC). The shortest sampling time of this ADC is 33 μs although we typically use it in the range of 100–500 μs per data point with 800–1000 total data points accumulated for each collision. The photocell device, which we previously used as our motion detector, is now used for

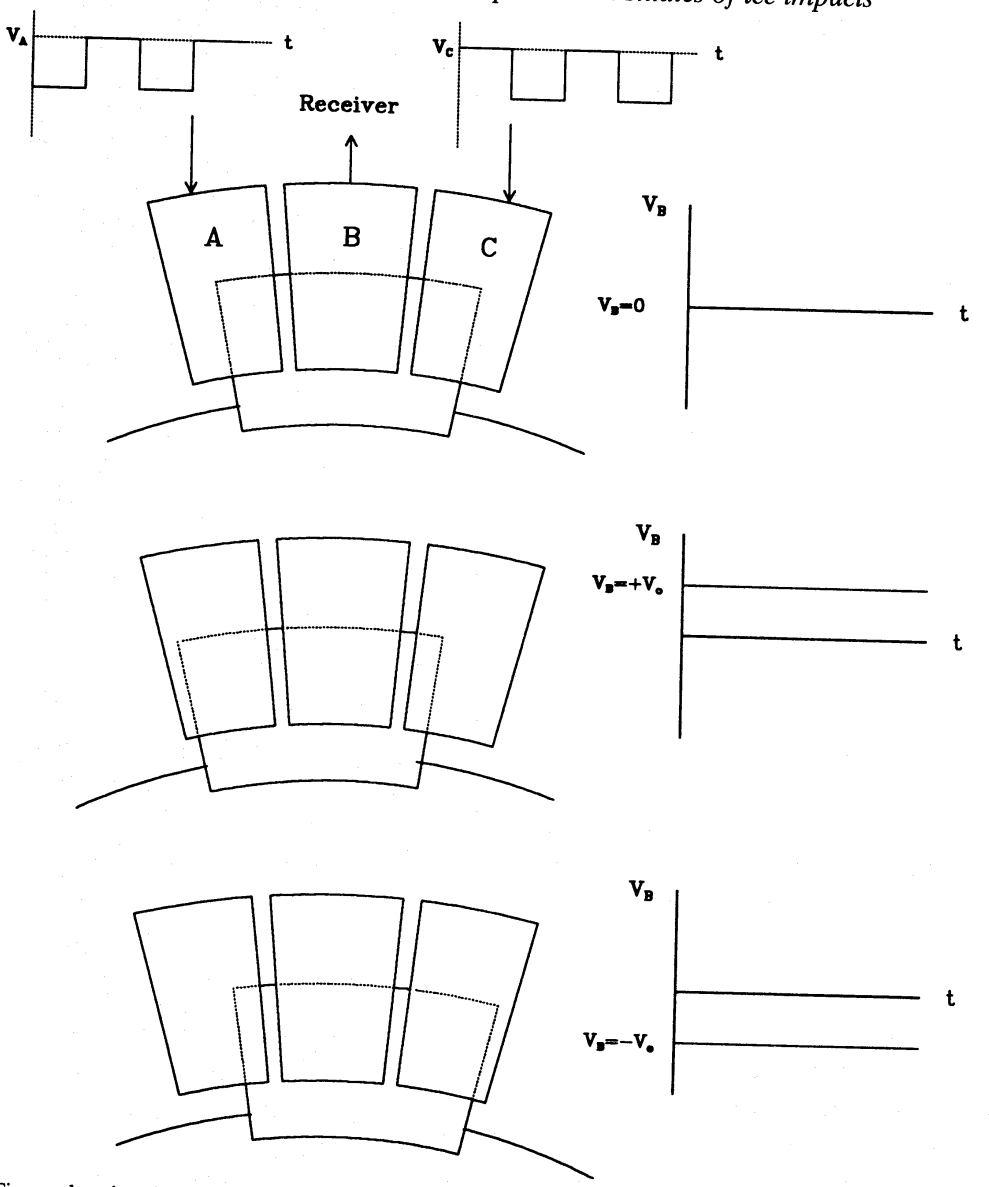

Figure 2. Figure showing the operation of the capacitive displacement device (CaDD). Plates labelled A, B and C are stationary and mounted on the copper can. A second set is attached to the pendulum. A square wave voltage is applied to Sections A and C (180° out of phase). In the top panel the pendulum is in its equilibrium position and the receiver plates, B, receive an equal amount of signal from plates A and C. The resulting voltage on B (V_B) is then 0. In the central panel the pendulum is displaced to one side so that the receiver detects more of the voltage signal on A. the resulting V_B in this case is $+V_0$. In the last frame the pendulum is displaced by an equal amount to the other side allowing the receiver to detect more of the waveform on C. The resulting V_B is $-V_0$.

providing a voltage flag for signalling the computer to commence reading the ADC. In this way data are acquired only during the pertinent time window encompassing the collision. We are thus able to obtain data on the displacement of the pendulum as a function of time during the entire collision. With this device we can obtain accurate measurements of the coefficient of restitution for velocities as low as 0.005 cm s^{-1} even for rather short periods of oscillation (10–15 s). This represents an order of magnitude improvement over the previous method for measuring the velocities.

Collisions are induced by use of an electromagnetic 'kicker'. This kicker consists of a small magnet mounted on the bottom of the disc in a horizontal position (see Fig. 1). When the

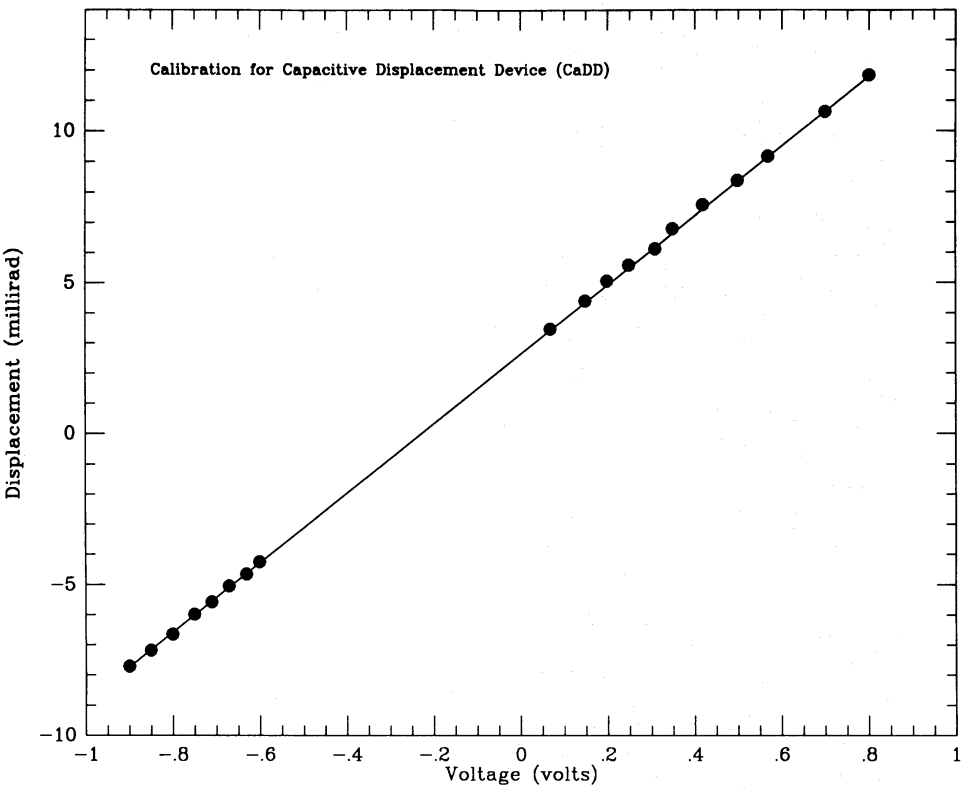

Figure 3. Calibration of the CaDD. This figure was obtained by measuring the voltage output of the CaDD as a function of known displacements of the pendulum. the displacements of the pendulum were measured using a laser beam reflected off a mirror on the pendulum axis.

pendulum is at its equilibrium position inside the cryostat, this magnet rests at the centre of a solenoid. A pulse of current through this solenoid produces an impulse to the magnet and hence initiates oscillation of the pendulum. By varying the amount of current flowing through the solenoid coils we can vary the size of the displacements and thus measure collision properties over a velocity range of 2 orders of magnitude (2–0.02 cm s^{-1}) during a given experimental run.

Ice particles were made using a spherical aluminium mould designed to freeze ice spheres with a radius of 2.5 cm onto an aluminium mount which can be directly attached to the disc pendulum. This mould provides spheres with a smooth surface as well as ensuring a uniformity in the size and shape for ice spheres used in different experimental runs. We were also able to examine the effects of the geometry of the contact surface by colliding spheres with larger radii of curvature. This was accomplished by using aluminium moulds which could freeze a different radius of curvature on the existing 2.5-cm radius sphere. This allowed us to increase the radius of the sphere without a concomitant increase in its mass and diameter. Moulds were machined so as to provide contact surfaces with a radius of curvature of 5, 10 or 20 cm.

The surface of the ice ball can be modified by sublimation and frosting. Sublimation was accomplished by evacuating the inner chamber at relatively high temperatures (200–220 K) thus allowing the ice sphere to sublimate. Sublimation is an excellent way to roughen a surface as the sublimation rate varies with lattice defects present at the surface. The resulting surface is criss-crossed with vary narrow wedges of ice. Frosting of the sphere was accomplished by a gas handling system which enables us to blow nitrogen gas saturated with water vapour across the contact surface of the ball thus allowing a layer of frost to form. During the frosting procedure the temperature of the cryostat increases slowly. For most of our experiments the ice ball tempera-

ture at which the frosting occurs is in the range of 130–150 K. Consequently, the frost should be primarily cubic (Whalley 1984).

Collisions of the ice sphere occur when it strikes a stationary ice brick mounted on a lead brick. The lead brick (mass=12 kg) provides enough inertia to ensure that no significant energy losses result from motions of the ice brick during the collisions. The lead brick rests on a platform which can be moved in a vertical direction. During the process of balancing the pendulum this platform is lowered so that the pendulum can swing freely. Once the pendulum has been balanced and the equilibrium (namely stationary point) established, the brick is slowly raised so that it just makes contact with the ice ball. This ensures that the ice sphere strikes the brick at the point of maximum angular velocity. Fig. 4 is a schematic of the experimental set-up showing the layout of the cryostat, laser, CaDD, and data-taking computer.

A typical experimental run proceeds as follows. The ice sphere is first cooled to about −20° C to prevent melting of the ice spheres during set-up stage of the experiment. The ice sphere is then attached to the disc pendulum and a crude balance of the system is achieved while the ice ball is under atmospheric conditions. These adjustments are made while the pendulum is in a styrofoam cryostat containing a nitrogen-rich atmosphere. Dry nitrogen gas is blown over the contact surface prior to and after placing the device into the main cryostat to remove microscopic frost particles. The pendulum is then cooled to about −40° C by feeding liquid nitrogen directly into the inner chamber of the cryostat. This direct cooling serves to lower the temperature of the ice sphere pendulum device quickly so as to prevent melting of the ice sphere while final adjustments are made on the apparatus. The rapid evaporation of the liquid nitrogen also serves to purge the system of atmospheric water and thus prevents the further accumulation of water frost on the ice sphere. The inner chamber is initially cooled by pouring liquid nitrogen via a feed-through at the top of the can. Additional cooling during the course of the experiment is provided by a liquid nitrogen bath which surrounds the outer wall of the cryostat. With this chamber we have been able to achieve temperatures down to 85 K with good temperature stability. A diffusion pump can also now be attached to the cryostat to provide a means for evacuating the inner chamber. At the present time we have been able to achieve pressures 10^{-4}–10^{-5} torr.

Final adjustments on the pendulum balance are made at this time using a glove box attached to the acrylic lid of the cryostat. This system greatly minimizes the amount of water frost which can accumulate on the surface of the ice particle and as a result we are able to collide much 'cleaner' balls than previously. The amount of frost which remains on the contact surface depends on the

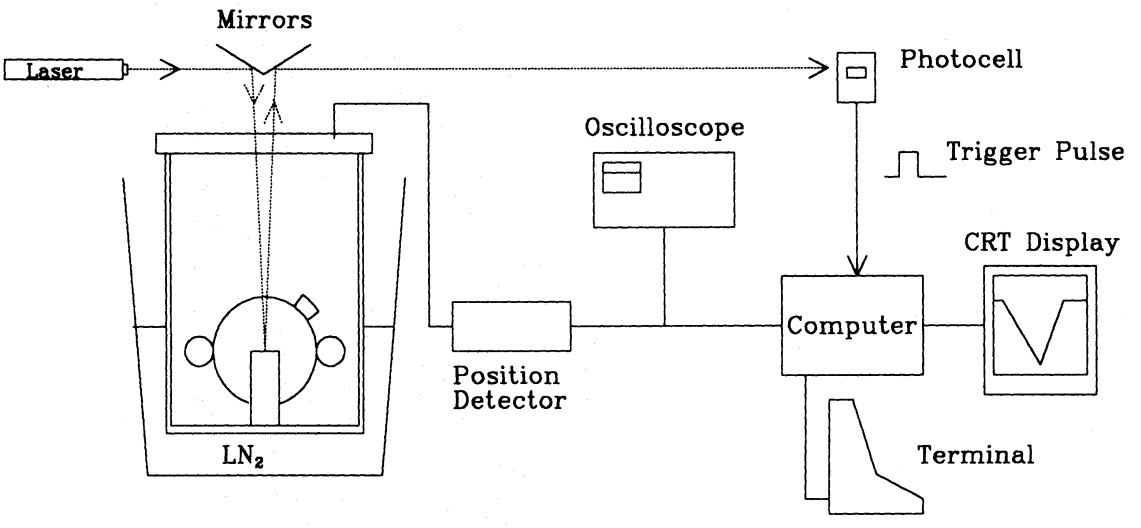

Figure 4. Schematic showing the layout of the experiment.

set-up time, the temperature of the ice sphere, and the amount of moisture in the air. Since this will vary between experimental runs, several runs have been made in order to average over this randomizing effect. After all adjustments are completed the apparatus is cooled to its operating temperature, typically 85 K, and evacuated with a diffusion pump to a pressure of about 10^{-2}–10^{-4} torr.

3 Experimental results

In Fig. 5 the position of the ball is shown as a function of time for a typical collision. Since the coefficient of restitution is defined by the ratio of the incoming and outgoing velocities, ε is calculated simply by the ratio of the slopes before and after the collision in this figure. Coefficient of restitution measurements were taken over several experimental runs and for ice spheres with radii of curvature of 2.5, 5, 10 and 20 cm. The data were collected at various temperatures ranging from 85 to 140 K. At these low temperatures there appears to be no significant effect of the temperature on the elasticity of the collision. This is demonstrated in Fig. 6 which shows data taken during two experimental runs (same radius of curvature) one at 90 K and the other at 145 K. The two data sets are consistent although we cannot rule out the possibility that the data set taken at the lower temperature have systematically higher values of ε. We note however, that there is a large scatter in the data points and a considerable overlap among the two data sets. As we shall demonstrate, the slight differences in ε can be accounted for by frost particles on the surface rather than a real tempeature effect. We also find that there is no trend with pressure as evidenced in Fig. 7. These data were taken during one run at a temperature of 110 K but at two different pressures, 760 and 10^{-2} torr. The differences between the two data sets are negligible. This indicates that our data should be applicable to Saturn's ring environment which is at a much lower pressure and possibly a lower temperature.

Fig. 8(a)–(d) show the resulting coefficient of restitution as a function of velocity for the four radii of curvature. The temperatures and pressures at which the data points were taken are

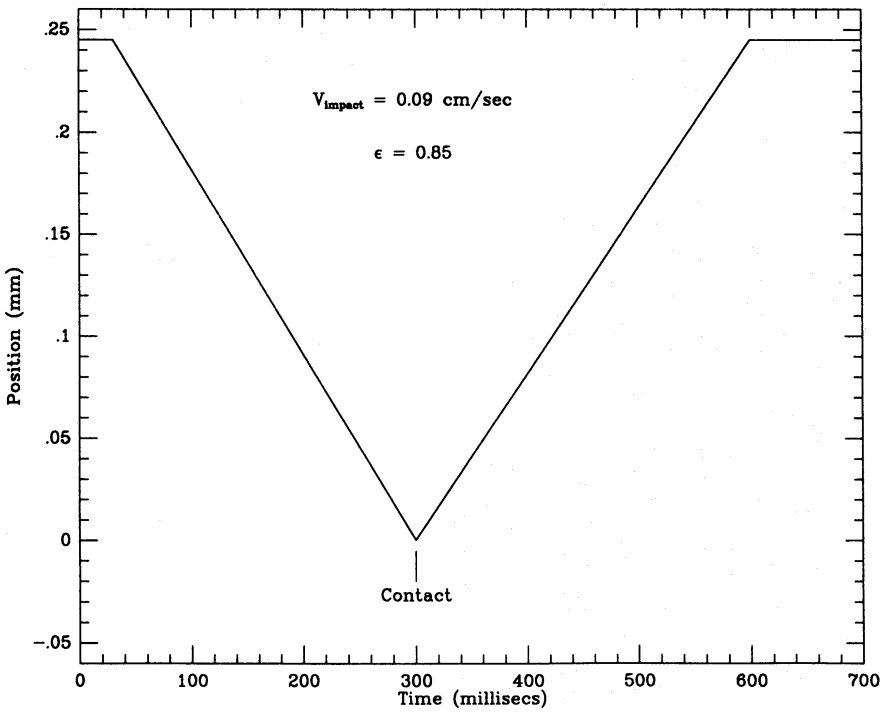

Figure 5. Typical output from the CaDD during a collision.

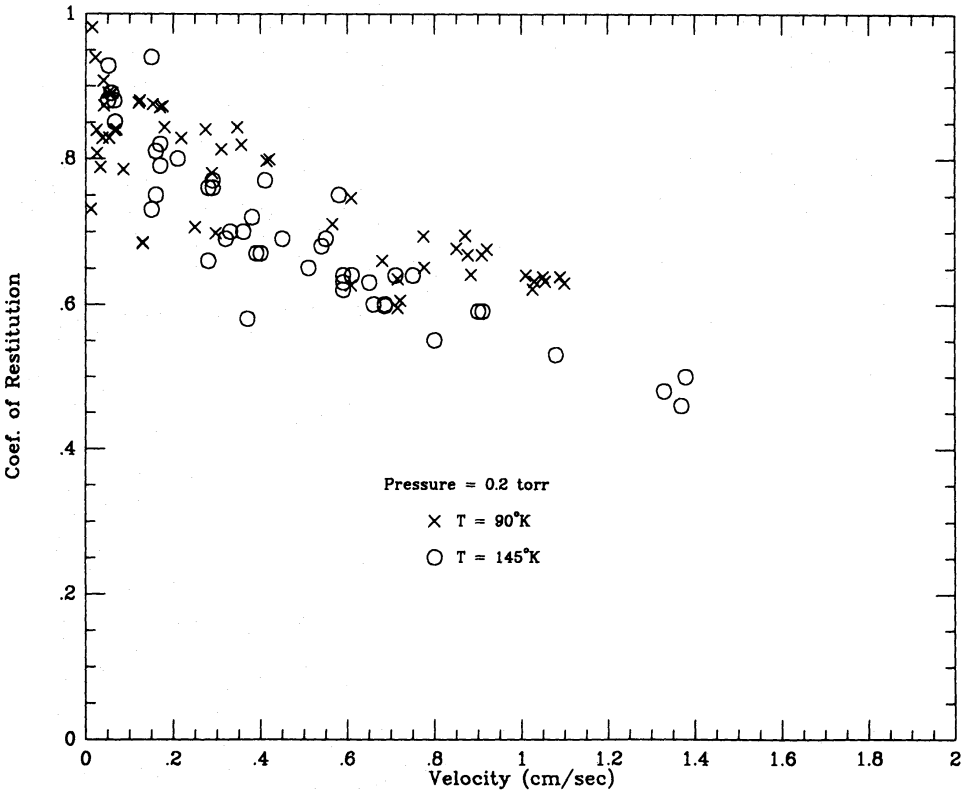

Figure 6. Data taken from two experimental runs using an ice sphere with a radius of curvature of 2.5 cm. The data were taken at the same pressure (0.2 torr) but different temperatures (90 and 145 K).

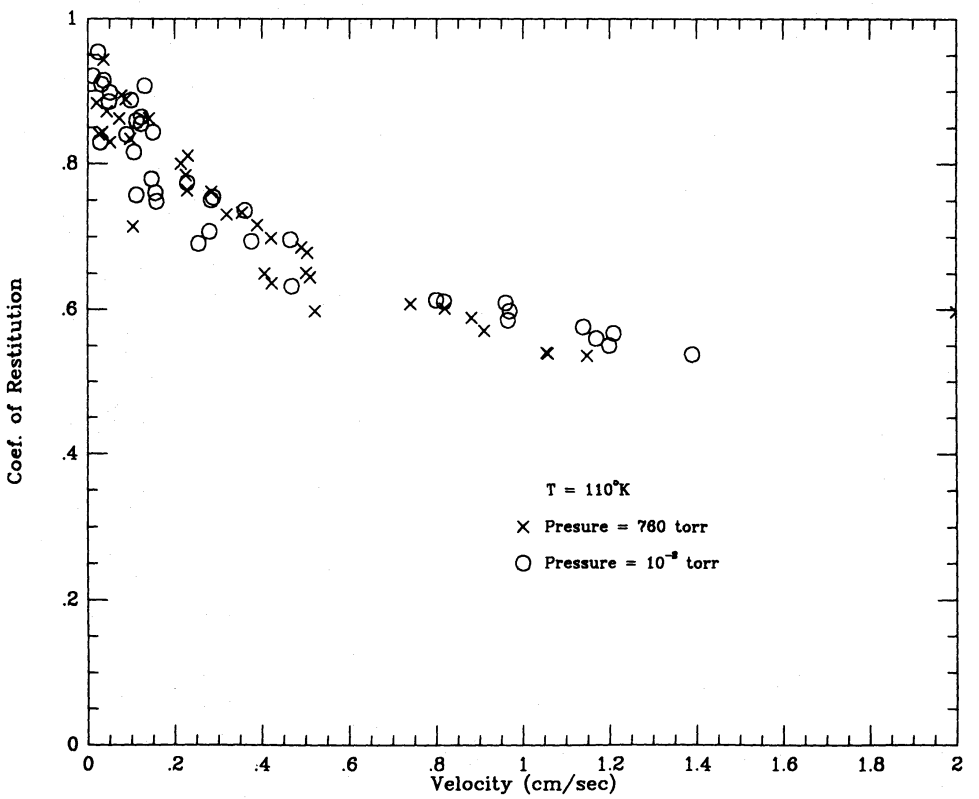

Figure 7. Data taken for the same ice sphere (radius of curvature =2.5 cm) at the same temperature but different pressures.

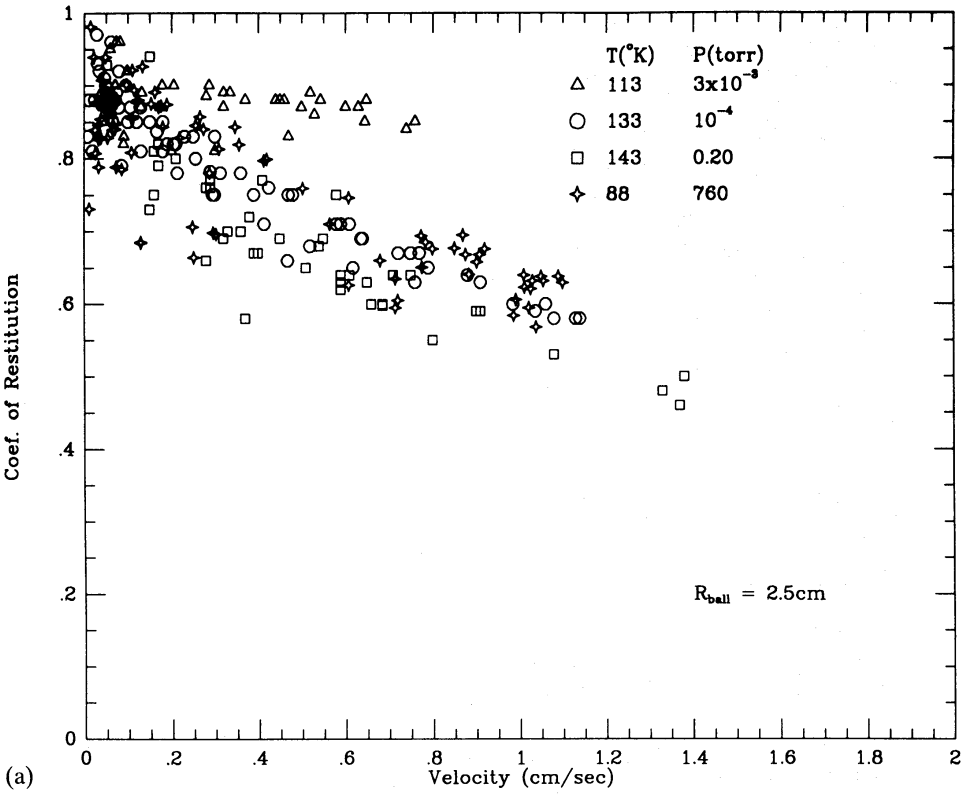

(a)

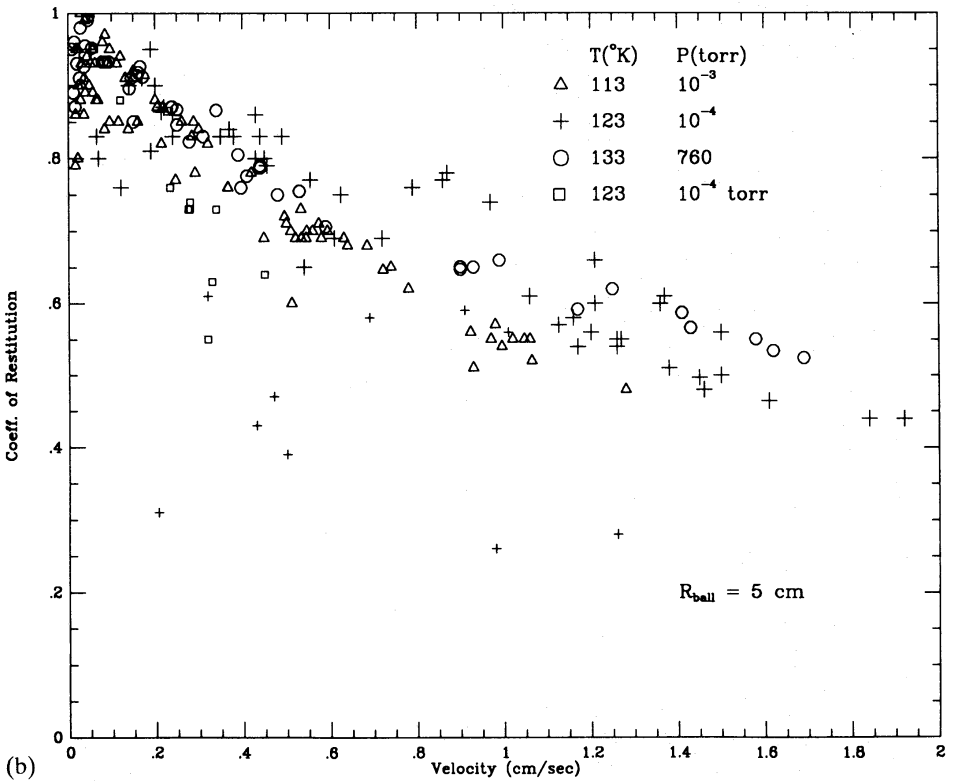

(b)

Figure 8. (a)–(d) Data taken from several runs using four different radii of curvature for the ice spheres (2.5, 5, 10 and 20 cm). The temperature and pressure at which the data were taken is indicated in each figure. Smaller symbols in Fig. 8(b) and (d) are data values from the first ten collisions of the ice sphere with the brick. These unusually inelastic collisions are interpreted as due to the presence of frost particles on the contact surface.

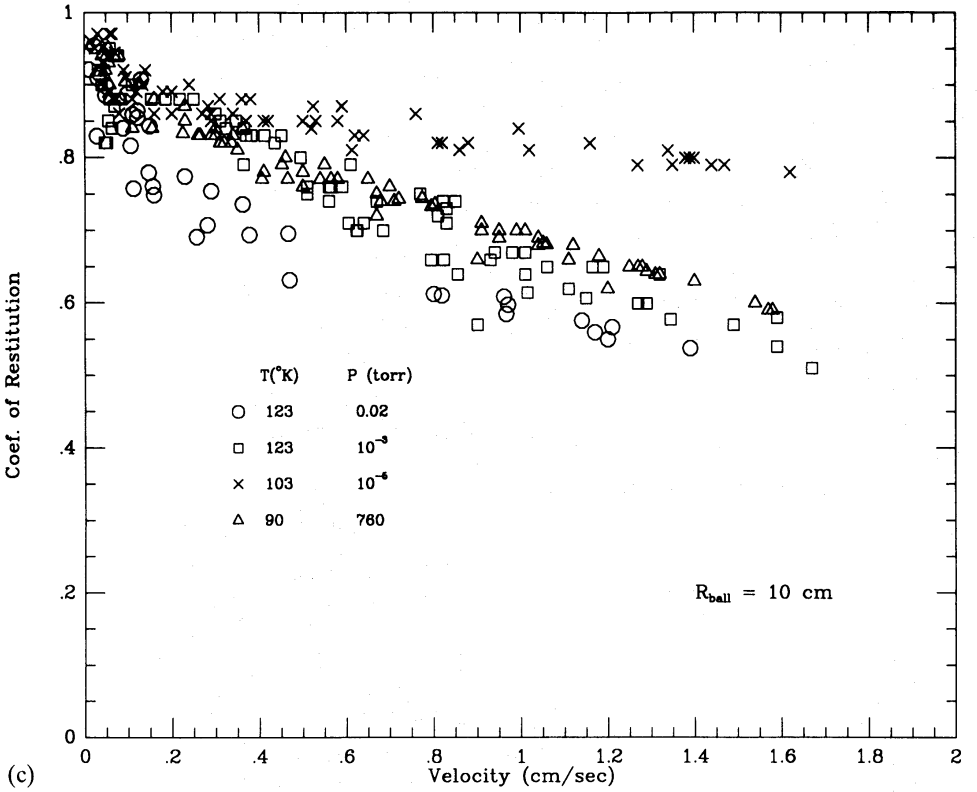

(c)

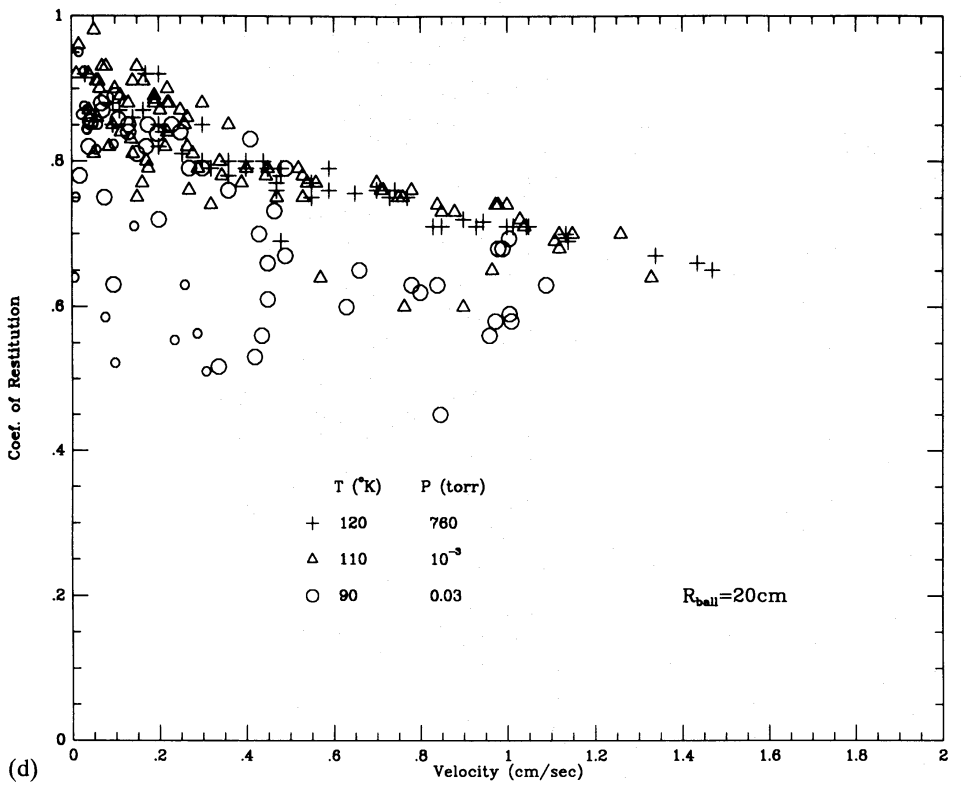

(d)

Figure 8–*continued*

indicated in each figure. Note that not only can there be large differences in $\varepsilon(v)$ between different spheres of the same radius of curvature but there is also considerable scatter among data points during the same experimental run and with the same ice sphere. The scatter cannot be due to experimental errors as these are quite small and in fact the error bars for most data points are comparable to the size of the plotted points. A similar amount of scatter was also evident in data taken with the old apparatus and presented in Paper I.

Since our experimental errors are too small to account for the scatter, it is likely to be associated with the crystal structure at the surface of the ice balls. A prime candidate for the cause of the scatter is the presence of small particles of frost on the contact surface which either formed during the preparation and transfer of the pendulum into the cryostat, or were produced during collisions. Further support for this assertion can be shown in Fig. 8(b) which shows a few, very inelastic collisions ($\varepsilon \sim 0.4$–0.6) with low impact velocities (less than 0.4 cm s^{-1}). Most of these data points were taken at the beginning of the run and represent the first few impacts after the apparatus had been cooled to its operating temperature. As the experiment progressed, each

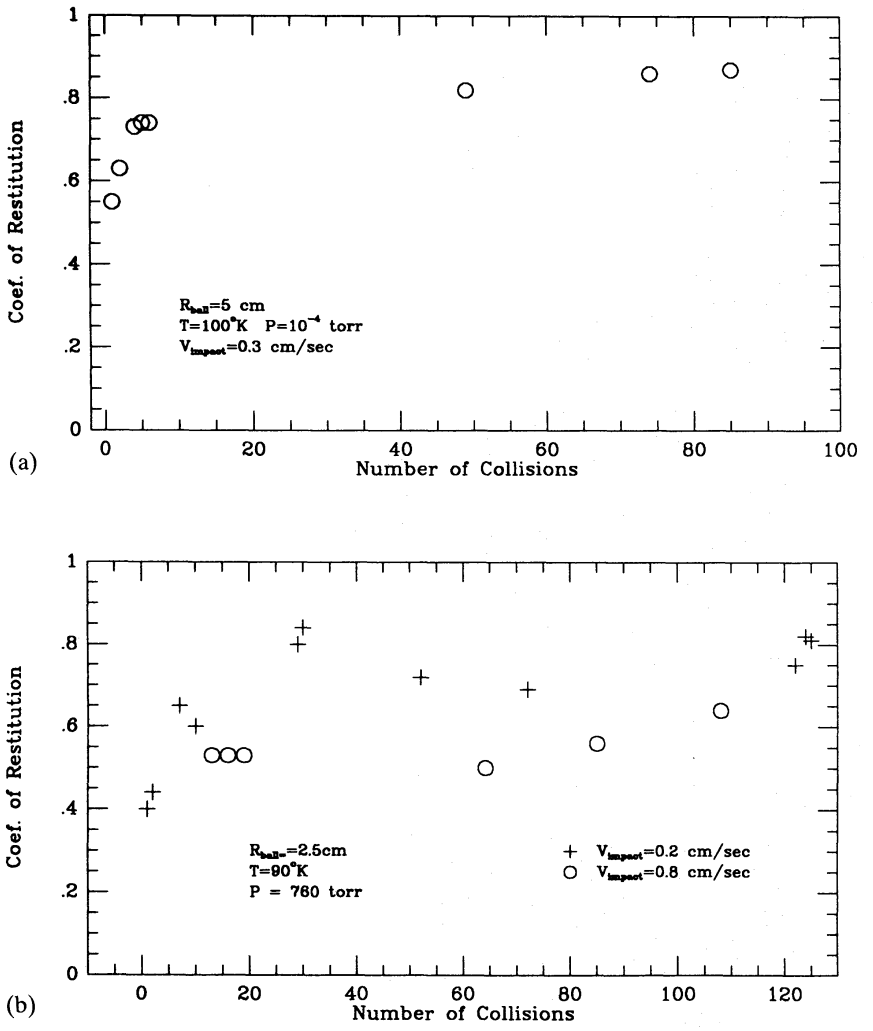

Figure 9. (a) The coefficient of restitution at an impact velocity of 0.3 cm s^{-1} as a function of collision number for a sphere with radius 5 cm. The collision number indicates the order in which the data were taken. The coefficient of restitution is low for the first few collisions due to the presence of frost particles on the contact surface. After a few collisions these particles become pulverized and ε approaches a nearly asymptotic value. (b) Same as in (a) except for a sphere of radius 2.5 cm and for two impact velocities. The coefficient of restitution rises even further after several high-velocity impacts.

successive collision (at a given velocity) would result in a higher coefficient of restitution measure. After several collisions (5–10) the coefficient of restitution would reach some asymptotic value and all subsequent measurements would cluster about a representative curve for that experimental run. We have attempted to illustrate this behaviour qualitatively by plotting the coefficient of restitution as a function of the number of collisions the ice sphere makes. Obviously the value of ε will depend on the impact velocity, so we have chosen to follow the change of ε for just a few selected impact velocities. This is shown in Fig. 9(a) and (b) taken from two data runs (R=5, 2.5 cm). We also noted the number of collisions the ice sphere had undergone previously and this is plotted along the abscissa. (This also indicates the order in which the data points were taken.) The first several collisions are rather inelastic but after several impacts the coefficient of restitution nearly reaches some asymptotic value.

Clearly this is indicative of a rough surface or the presence of microfrost particles on the contact surface. The first few collisions are highly inelastic because energy is expended in pulverizing these particles or breaking off the high points of the surface. After many collisions the fracturing process saturates and additional collisions result in little further damage of the particles. The energy losses at this point are now likely due to the compression of the thin layer of frost and brittle fracture of the ice sphere itself. If this scenario were true then we would expect high velocity impacts to be more efficient at pulverizing the frost layer and this appears to be the case. Referring to Fig. 9(b) note that for the first few impacts (at V=0.2 cm s^{-1}) the coefficient of restitution rises quickly from 0.4 to 0.6. After this several collisions were made at impact velocities of 0.8 cm s^{-1} before making additional measurements at the original impact velocity of 0.2 cm s^{-1}. These additional measurements yielded restitution measures significantly higher than before, indicating that the high impact collisions provided additional pulverization of the frost layer.

3.1 CONDITION OF THE CONTACT SURFACE

The fact that the presence of frost particles can induce large changes in $\varepsilon(v)$ suggests that the dominant factor determining the coefficient of restitution for ice spheres is the physical condition of the contact surface rather than the radius of the sphere. To further examine this effect we chose to alter the contact surface for the same ice sphere taken during one experimental run via the process of sublimation and frosting as discussed in Section 2.

Fig. 10(a) represents data taken for an ice sphere with a radius of curvature of 20 cm with three different conditions of the contact surface. The circles represent data taken when the sphere was relatively smooth and free from frost particles. We then evacuated the inner chamber and allowed sublimation to roughen the contact surface. We estimate that approximately 0.5 g of ice were removed from the sphere, although this value is highly uncertain. The resulting values of the coefficient of restitution are significantly lower than when the sphere is smooth. In particular, the first few collisions are often very inelastic. We then used our gas handling system to deposit a layer of frost 10–30 μm thick on the contact surface. The resulting restitution measurements are indicated by crosses. The presence of frost on the contact surface results in further reduction in the coefficient of restitution. Fig. 10(b) shows data taken in the same manner but for a sphere with a radius of curvature of 5 cm. The first few collisions when the sphere was clean were very inelastic (ε~0.2–0.4) due to the presence of frost on the contact surface which accumulated during the transfer process. Note that many of these points lie very near the typical $\varepsilon(v)$ for frosted and sublimated spheres. After several collisions the subsequent restitution measures had more typical values as defined by the upper envelope of points. Sublimation and frosting of the sphere not only lowers the overall $\varepsilon(v)$ curve but can also introduce considerable scatter in the measured data values.

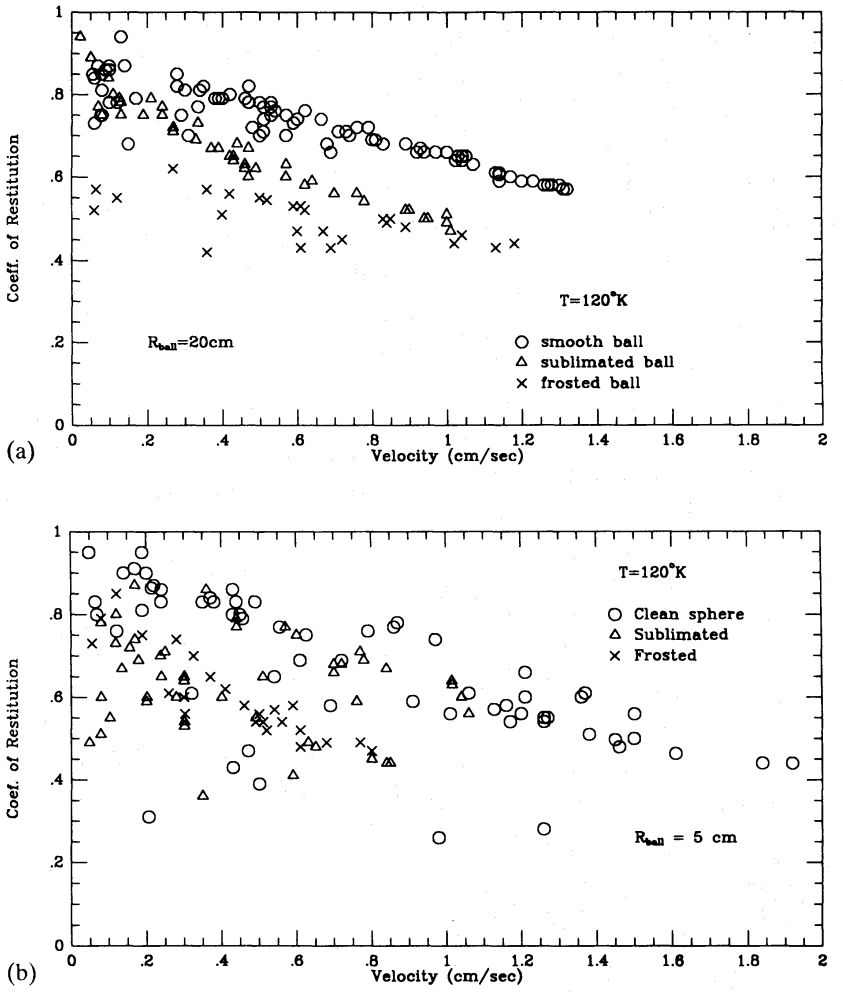

Figure 10. (a) and (b) Figure demonstrating how the condition of the contact surface can greatly alter the resulting restitution measures. The coefficient of restitution for two spheres (radius of curvature=20, 5 cm) and with different surface conditions. In each case measurements were first taken using a smooth sphere (circles), then data were collected after the surface was roughened by sublimation (triangles), and finally the surface of the sphere was covered with a layer of frost before taking the final measurements (crosses).

3.2 SMOOTH ICE SPHERES

We have shown in the previous section that a roughened or frost covered contact surface can significantly alter the value of ε at a given velocity (by up to 40 per cent). Ideally one would also like to know the form of $\varepsilon(v)$ for a smooth, very clean ice sphere. Fortunately we were able to take such data during two experimental runs, one for an ice sphere with R =2.5 cm and another with R=10 cm. These two runs were exceptional in that virtually no frost was able to form on the ice spheres during the set-up procedure. This was accomplished by keeping the ice spheres just below freezing (−10°C) during the set-up. Also the process of attaching the ice sphere to the pendulum, achieving a rough balance, placing the device into the cryostat and cooling to −30° took less than 5 min in both cases. The relatively warm temperature of the ice sphere coupled with the short set-up time gave frost particles little opportunity to form on the surface of the ice ball. What few particles may have formed were blown free using dry nitrogen just before placing the pendulum into the cryostat. Removal of these ice particles from the cryostat confirmed the cleanliness of these spheres as there was no evidence for compacted frost at the contact surface. Also the texture of each of the balls was quite smooth with a feel that could best be described as

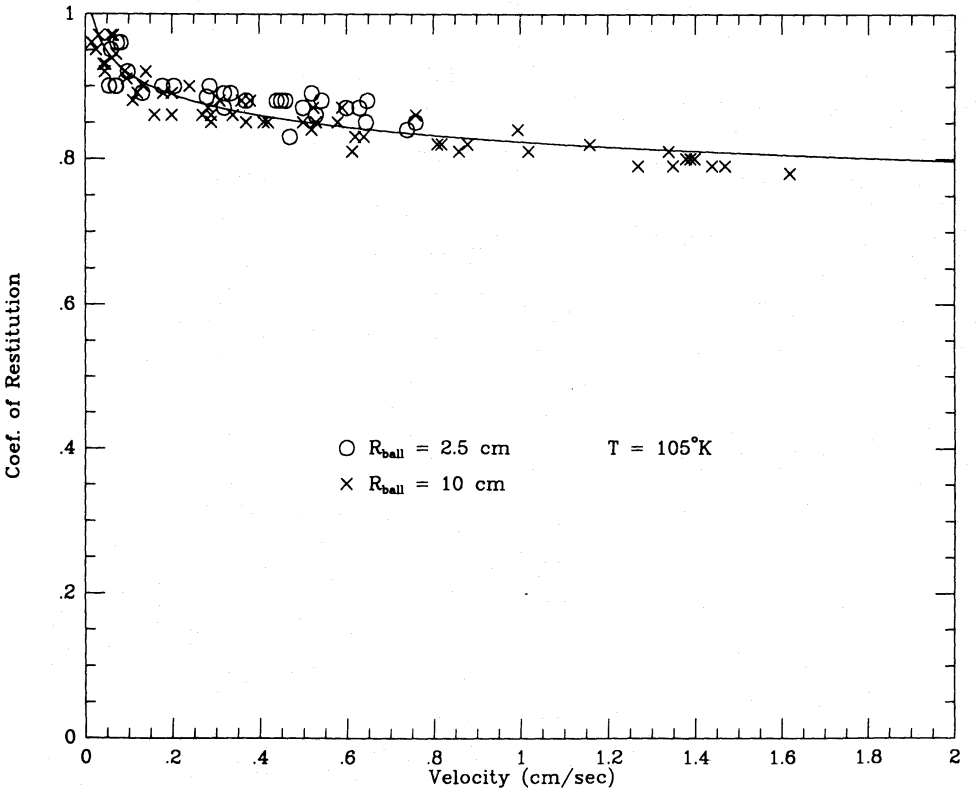

Figure 11. Coefficient of restitution as a function of velocity for two very smooth spheres and with two different radii of curvature (2.5 and 10 cm). The line drawn represents a power-law fit to the data.

that of polished marble. Fig. 11 shows the $\varepsilon(v)$ data for these two spheres. The data are surprising in three respects. First, the spheres are much more elastic than the highest values of more typical data (by about 20 per cent at v=0.6 cm s^{-1}). Secondly, the velocity dependence is much flatter than our more typical measurements. In fact in the velocity range 0.2–0.8 cm s^{-1} the value of the coefficient of restitution only changes from 0.9 to 0.83. (Note: the fact that these very smooth spheres have a much higher restitution measure than typically measured suggests that energy losses due to deformations of the pendulum system are indeed negligible as we stated earlier.) Lastly there is no noticeable difference in $\varepsilon(v)$ between the two spheres suggesting that the radius of curvature for smooth spheres plays a negligible role in determining the elasticity of a collision. This suggests that any differences in $\varepsilon(v)$ among the different size ice spheres for our more typical measurements must result from the effects of the thin layer of pulverized particles on the contact surface.

3.3 EMPIRICAL FITS TO THE DATA

In the absence of a good theoretical model for the loss mechanism, one would like to obtain an empirical fit to the coefficient of restitution which includes the dependence on the velocity as well as the radius of curvature, R. As we have demonstrated earlier, large changes in $\varepsilon(v)$ can be induced by different conditions of the contact surface and this can obscure any dependence on R. In fact the data on smooth spheres indicate that there is little dependence on the radius of curvature and any functional dependence we find with R includes the effect of small amounts of pulverized microfrost particles on the contact surface.

Although there can be large variations in $\varepsilon(v)$ for different ice spheres with the same radius of curvature, typical data values tend to cluster about a representative curve for that radius and it is

this curve for which we shall seek an empirical fit. In finding a fit to $\varepsilon(v)$ we tried several functional forms. The first, most obvious choice was a power law of the form $\varepsilon(v)=Cv^{-b}$ since this provided an excellent fit to the data presented in Paper I. To our surprise we found that this form provided a poor fit to most of the data regardless of the radius of curvature. Alternately we tried an exponential law of the form $\varepsilon(v)=C\exp(-\gamma v)$ and found that it provided an excellent fit for most data points in the range $0.2<v<1.5$ cm s^{-1}. A least-squares fit of this form was then found for each experimental run using data values in the above velocity range. Average values of the parameters C and γ for each radius of curvature were then computed. Care was taken to avoid using in the fits those data points which exhibited unusually low values of ε (compared to typical values obtained in the run) in that these were atypical data values probably due to the presence of large ice chips at the contact point of the ice sphere for the first few collisions. Fig. 12(a) and (b) show the resulting behaviour of C and γ as a function of radius of curvature. There appears to be very little change in the value of C with increasing radius of the particle. There is however a noticeable tendency for γ to decrease with increasing radius. The behaviour of γ with radius of curvature can be fitted quite nicely by the linear form $\gamma(R)=-0.01R+0.41$, where R is the radius of the ice sphere in cm. We can thus combine the velocity and radius of curvature dependence of ε into one convenient form namely

$$\varepsilon(v,\ R)=0.90\ \exp\ [-(0.01R-0.42)\,v]. \tag{1}$$

This is an adequate description of the coefficient of restitution for different size ice spheres with a thin layer of compacted frost on the surface.

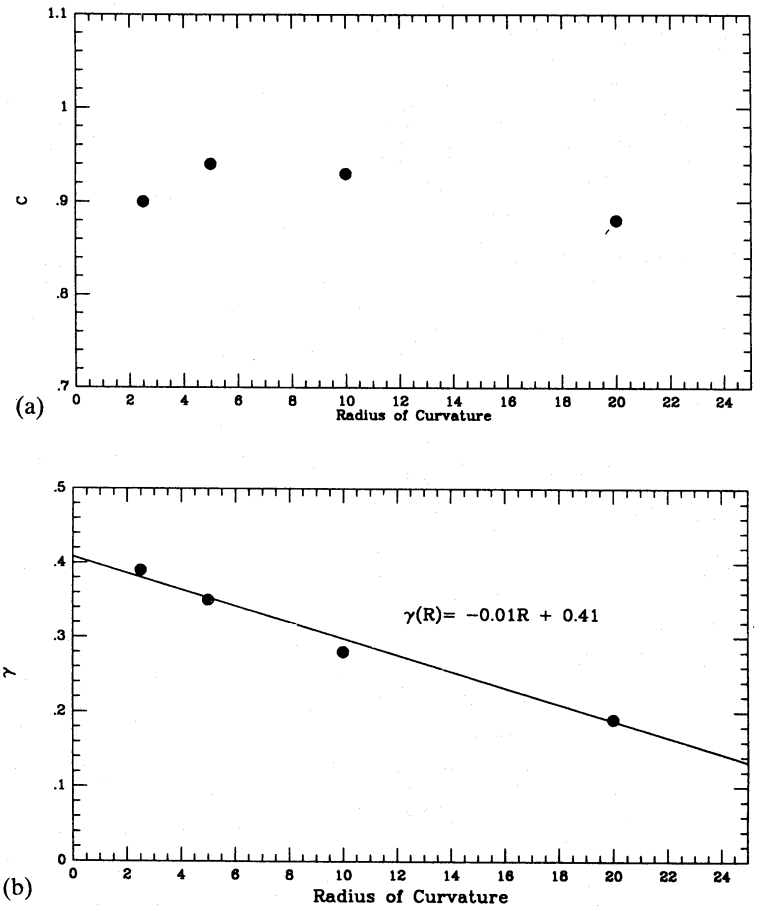

Figure 12. Behaviour of the parameters C and $\gamma[\varepsilon(v)=C\exp(-\gamma v)]$ as a function of radius of curvature.

Although the exponential form provides an adequate fit in the velocity range $0.2<v<1.5$ cm s^{-1} it was unable to account for the sharp rise in ε below 0.2 cm s^{-1} which was observed for many experimental runs. Fig. 13(a)–(d) shows an example of this behaviour for each radius. Each figure represents data taken from one experimental run for which the ice sphere had a minimum of accumulated frost. (The fact that these spheres had small amounts of accumulated frost was corroborated by the high values in ε exhibited from the first few collisions as well as the relatively small amount of scatter of the data points about a representative curve.) To account for this steep rise a power law of the form $\delta\varepsilon=Dv^{-b}$ was added to the exponential form previously determined. A reciprocal power law was chosen since it has the nice features of providing a sharp increase in ε at low velocities, yet contributes little to the restitution coefficient at the higher velocities, which should be dominated by the exponential form. This obviated the necessity of only including this form for the low velocities. The power law could simply be added to the exponential form thus yielding a form of $\varepsilon(v)$ valid for all velocities. Table 1 lists the values of the parameters D, and b for each radius of curvature. The resulting fit to the data using the sum of the two mathematical forms are shown as lines in Fig. 13(a)–(d).

Unfortunately this exponential form for $\varepsilon(v)$ is unable to fit the data obtained for very smooth, clean balls as exhibited in Fig. 11. For this data a power law of the form $\varepsilon(v)=0.82v^{-0.047}$ provided an adequate fit in the velocity range $0.02<v<1.5$ cm s^{-1} for both the 2.5-cm radius sphere as well as the 10-cm radius sphere. The fact that the same mathematical form can adequately fit both size spheres again suggests that for smooth spheres there is very little dependence of ε on the radius of curvature. Thus, an understanding of the dependence of $\varepsilon(v)$ on R presented earlier must also include the effects of a thin layer of pulverized loose ice particles on the surface as well as the geometry of the contact surface.

3.4 DISCUSSION OF ERRORS

As stated earlier the errors in this experiment are generally small due to the improved method of measuring the velocities. A more detailed discussion is in order here. The errors in the measured velocity are primarily due to errors in the calibration of the CaDD (from voltage to displacement) and the error in measuring the distance of the contact surface from the axis of the disc (this is needed to convert angular velocity to linear velocity). As demonstrated earlier the CaDD is a very linear device and errors imparted by uncertainties in the calibration are no more than 0.5 per cent. The distance to the contact point can be measured to within an accuracy of 1 per cent resulting in a total error for the measured velocities of no more than about 1.5 per cent.

In determining the error in the coefficient of restitution, uncertainties in calibration of the CaDD are not as important because we take the ratios of two very well determined slopes and the conversion from angular displacement to velocity need not be applied. This error can be neglected. A more important source of error, particularly for the low velocity impacts, are the small vibrations of the apparatus which can impart energy to the ice sphere during the collision. Depending on the phase of the ice sphere's motion with respect to the vibrations, the resulting coefficient of restitution can be either higher or lower than if no vibrations were present. In order to minimize these vibrations, we place the cryostat on a table whose feet rest on vibration pads. All measurements are made with all mechanical vacuum pumps in the laboratory off. We also found that the presence of an evaporating reservoir of liquid nitrogen surrounding the outer can of our cryostat was also a significant source of vibrations. Efforts were made to keep this reservoir empty during low impact velocity measurements.

To measure the amount of noise due to room vibrations we allowed the ice sphere to undergo several collisions starting from a very small amplitude (<0.003 cm) and collected data over a long time-base. In this manner we were able to monitor many tens of collisions and measure the

velocities before and after each collision. We found that for these low velocity impacts ($\sim$0.001 cm s^{-1}) that about half of the collisions resulted in the ice sphere gaining energy from the impact ($\varepsilon>1$). This is what we would expect from the presence of random vibrations. Half of the time an ice sphere should gain energy and half of the time its resulting energy would be lower than what it would have been in the absence of vibrations. For those collisions resulting in an ε greater than unity we determined that the average velocity imparted to the ball is 7.5×10^{-4}cm s^{-1} with a standard deviation of 6.5×10^{-4}cm s^{-1}. The largest velocity imparted to the ice sphere during a collision is about 0.002 cm s^{-1} but this occurs for only about 3 per cent of the collisions. These room vibrations thus introduce an error of about 5 per cent in the coefficient of restitution for our lowest velocity data points presented ($v\sim$0.015 cm s^{-1}) and is less than 1 per cent at a velocity of 0.1 cm s^{-1}.

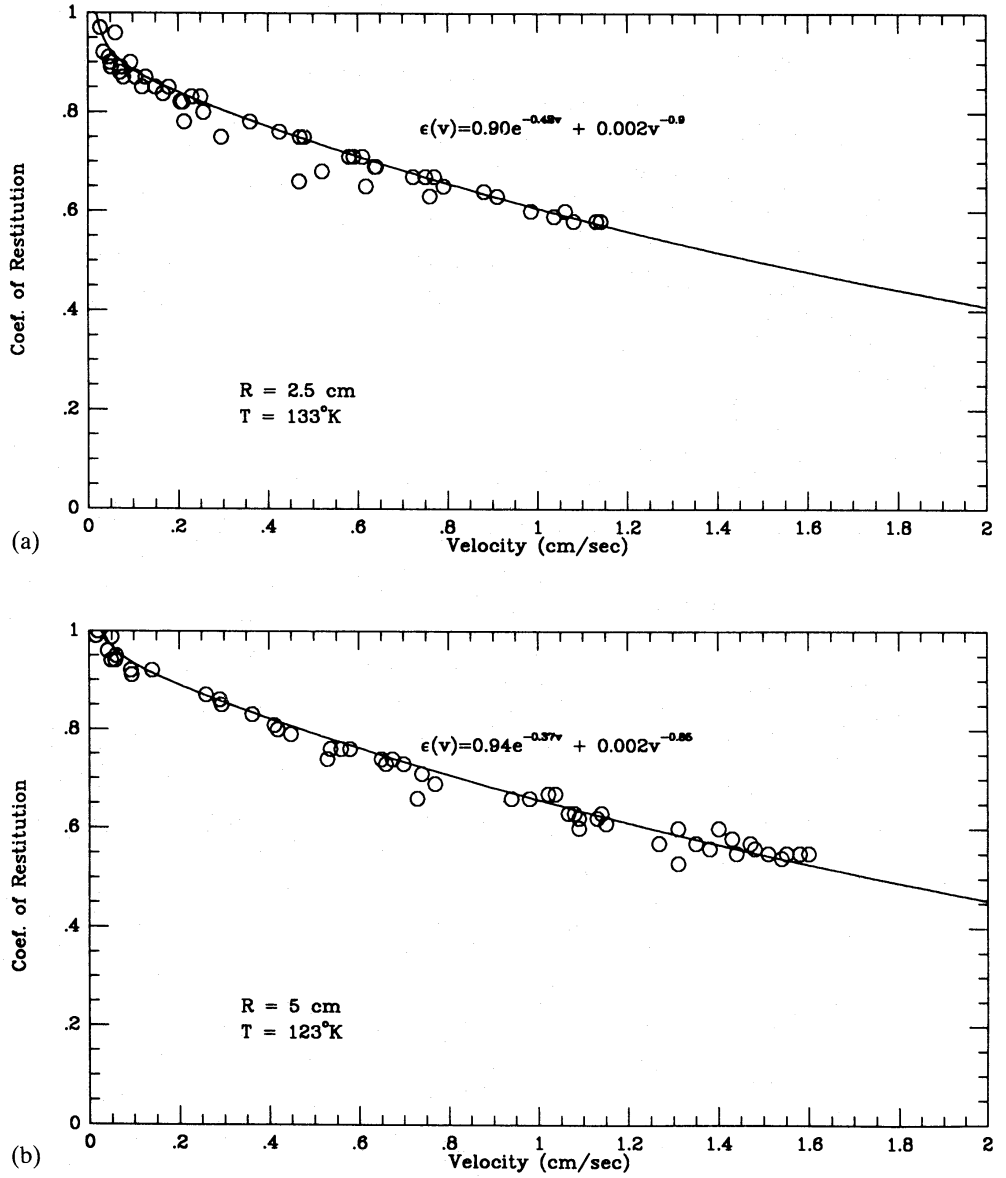

Figure 13. (a)–(d) Empirical fits to the coefficient of restitution for selected runs at each radius of curvature. The mathematical expression used for each fit was of the form $\varepsilon(v)=C\exp(-\gamma v)+Dv^{-b}$. In making these fits data points from the first 10–15 collisions were not used as these are usually more inelastic than more typical values due to the presence of frost particles which accumulated during the set-up procedure.

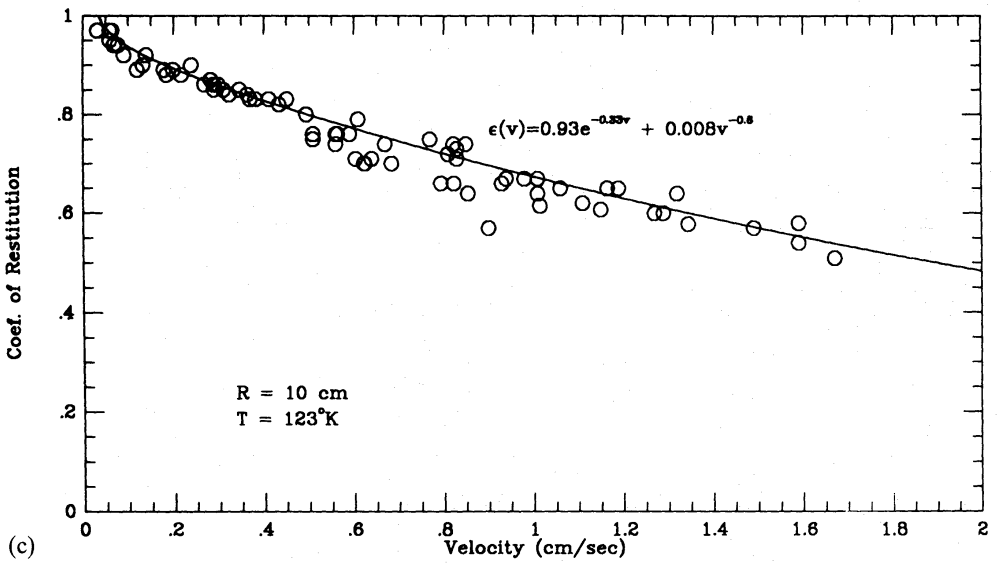

(c)

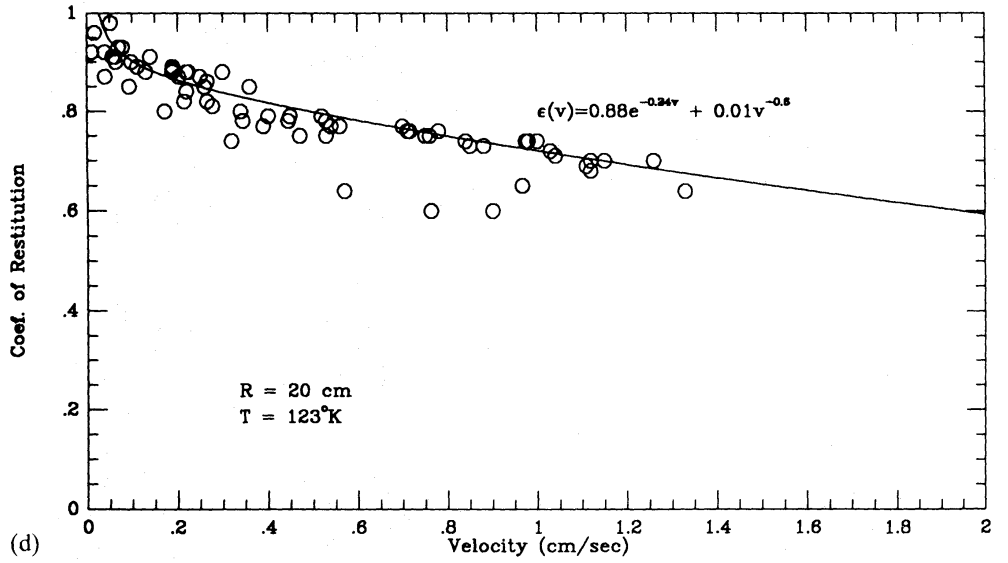

(d)

Figure 13–*continued*

Table 1. Parameters for $\delta\varepsilon = Dv^{-b}$.

Radius (cm)	D	b
2.5	0.002	0.9
5	0.002	0.9
10	0.008	0.6
20	0.01	0.6

3.5 DISCUSSION OF RESULTS

Data presented in this paper differ from those presented in Paper I in two significant areas: (i) typical values of ε at velocities greater than 0.05 cm s^{-1} are higher (by about a factor of 2) compared with the data taken with the old apparatus, and (ii) the typical behaviour of ε with velocity for the present data can be best described by an exponential velocity law of the form $\varepsilon(v) = C \exp(-\gamma v)$ ($\gamma \sim 0.4$) whereas the old data were best fitted by a power law of the form

$\varepsilon(v)=Av^{-b}(b\sim1/4)$. The disparity of the two results can be accounted for by differences in the surface conditions and the temperature of the ice spheres used in the two experiments. In fact for data taken for more heavily frost-covered ice spheres with the present device we are able to recover the previously obtained power law relationship thus dispelling any doubts that the effect is due to differences in the two apparatuses.

Fig. 14 represents restitution data for frosted spheres combined from several runs at a temperature of about 120 K (circles). The solid line through the points represents a power-law fit to the data of the form $\varepsilon(v)=0.48v^{-0.20}$. (Although an exponential law does provide a slightly better fit, the power law is also consistent with the data to within the scatter of the data points.) This velocity behaviour is very similar to that determined in Paper I (indicated by the second line), the only exception being that it is displaced slightly towards higher values of ε (this is just a reflection of the constant in front of the velocity term being 0.48 as opposed to 0.32). However, for similar data taken at higher temperatures, this apparatus produces a velocity dependence in ε that is consistent with our previous results in that a power law indeed provides a better fit to the data over an exponential law. We thus conclude that our previous results are valid for ice spheres covered with a layer of frost and at temperatures ~200 K.

4 Conclusions

The results presented in Figs 8–11 clearly indicate that the collisional properties of ice particles are sensitively determined by their surface structure. Although we do not have any direct data on the surface structure of the ice particles in planetary rings, some useful constraints may be

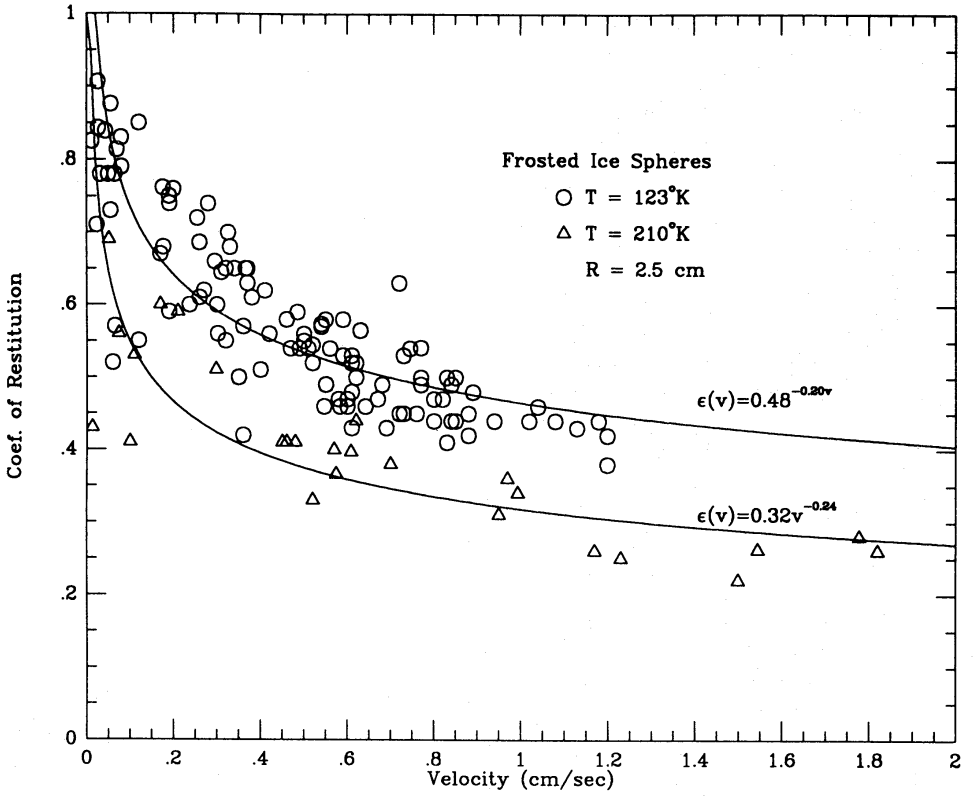

Figure 14. Empirical power law fit to frosted spheres (R=2.5 cm) at two temperatures (123 and 210 K). Also shown is the empirical fit determined in Paper I (lower line).

inferred from *Voyager's* data on the thickness of the ring, density wave structure near resonances of perturbing satellites, and our present experimental results.

Our data indicate that if the surface of ring particles is very smooth, such that it is primarily made of regular crystalline ice, the collisions would be very elastic even at relatively large impact velocities (see Fig. 11). In this case, the collisions are not sufficiently dissipative to allow evolution towards kinematic equilibrium in the rings unless the optical depth, τ, is greater than about 0.8 (Fig. 16). Thus, the rings' thickness would become considerably thicker than a few hundred metres which is not consistent with the *Voyager's* data (Cuzzi *et al.* 1984).

Alternatively, if the surface of the ice particles is covered with frost with a thickness greater than a few μm or densely populated with fractures and dislocations induced by thermal stress or collisional effects, the collisions would be very dissipative for relatively low impact velocity (Fig. 10a and b). In this case a lower ε would lead to a lower dispersive velocity. Consequently for density waves launched at certain known resonances of satellites, the dispersive motion within the wave trains would be effectively damped very close to the position at which the waves were launched. Therefore these waves would propagate to much longer distances (Shu *et al.* 1986). This again is inconsistent with *Voyager's* data (Cuzzi *et al.* 1984).

While these considerations provide some useful constraints on the surface structure of ice particles in planetary rings, the physical processes which regulate the resurfacing of the particles are poorly known. Our experimental results (Fig. 9) indicate that repeated direct impacts, with relatively low velocities, over a given spot can compress frost and loose chips in that region against the bulk of the ice particle. Consequently, the surface becomes smoother and the coefficient of restitution increases. We also note that large-velocity, direct impacts do not lead to even more elastic collisions for such cases. Presumably there is a limit to the extent of compaction. Relatively high-velocity collisions may fracture the surface and knock off chips at the same time as they compress the material on the surface, thereby minimizing any smoothing processes.

In addition to erosion due to direct collisions (Marouf *et al.* 1983), fractures and dislocations may also be induced at the surface of ice particles through charged particle or micrometeorite bombardment (Durisen 1984). In addition, the ice particles in planetary rings continually experience ambient temperature variation which may cause considerable thermal stress (Borderies, Goldreich & Tremaine 1984). Such thermal processes may lead to considerable sublimation. While all of these processes may cause minor changes in the mass of the particles over a long period of time, they can introduce sufficient irregularities to the surface of the ice particles that the collisional properties of the particles can be significantly altered on a relatively short timescale (Figs 9 and 10). Changes in the collisional properties would in turn lead to changes in the viscous evolution of the ring system.

Another factor that contributes to the surface structure of the ring particles is the accretion of eroded debris. This process is probably very efficient at introducing frost on to the surface of the particles. Our experimental results again indicate that this effect would cause the collisions to be more dissipative. Whether this is an important process in regulating the dynamical evolution of the ring system depends on whether the fresh frost/chip layer can form at a faster rate than the rate at which it is being compressed through direct collisions.

In a realistic analysis of the ring dynamics, these surface effects must be taken into consideration because they all lead to significant changes in the subsequent kinematic properties of the ring particles. For example, we note that in the regime in which the surface structure of the particles is neither artificially smooth nor densely populated with fractures or fresh frost, there is still a large range in the coefficient of restitution at a given impact velocity (especially in the range relevant to planetary rings) . This spread in the coefficient of restitution, which is independent of the environmental temperature or pressure, can induce a dispersion in the collisionally induced viscous stress at any given velocity. If the ring particles are in a state of kinematic equilibrium, this

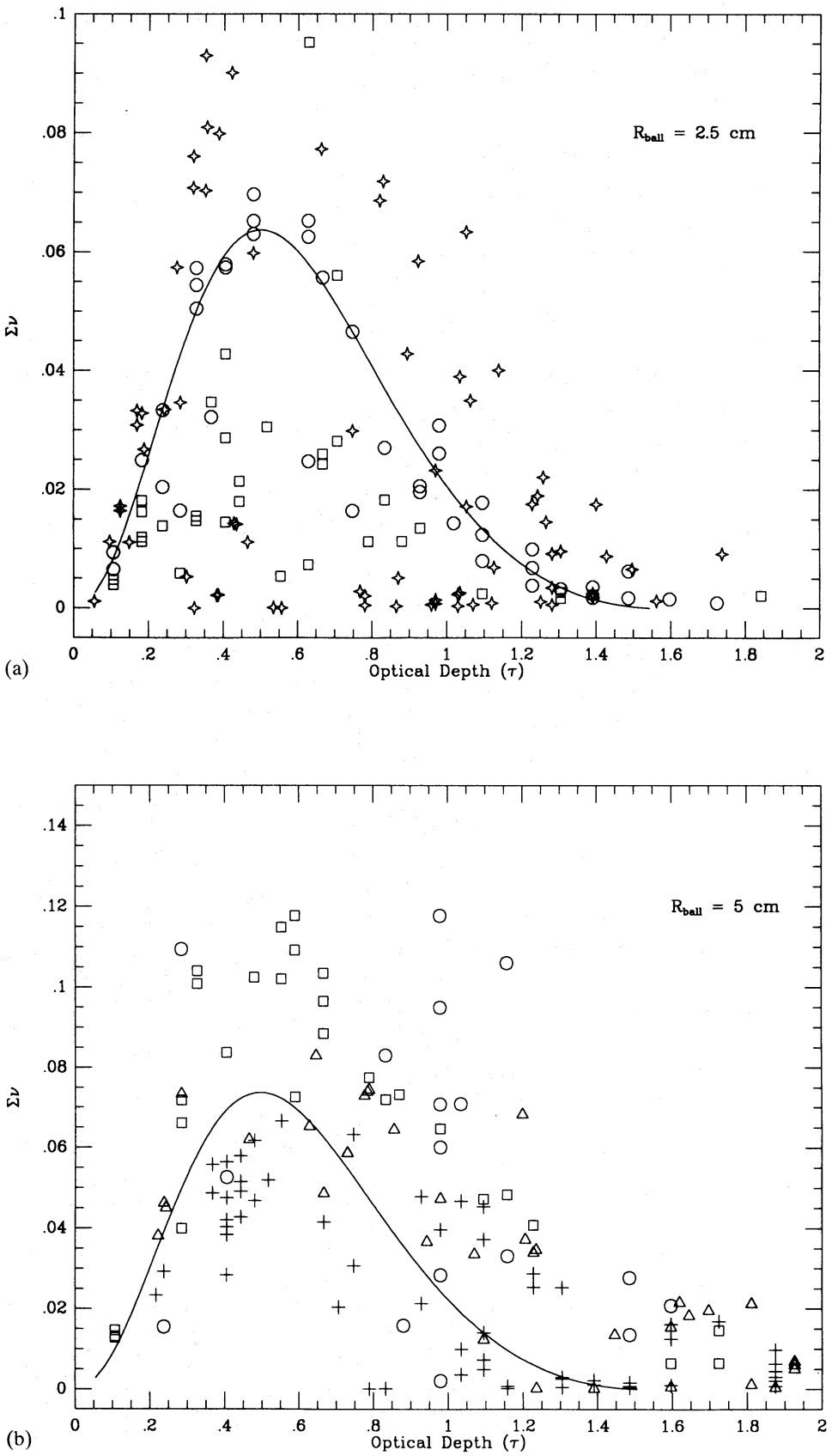

Figure 15. (a)–(d) The viscous couple $\Sigma\nu\,[=\tau^2\upsilon^2/(\tau^2+1)]$ as a function of optical depth (τ) for the radii of curvature used in this experiment. The line represents values computed using the empirical relationships for $\varepsilon(\upsilon)$ and equations (2) and (3). Symbols represents the same experimental runs as in Fig. 8(a)–(d).

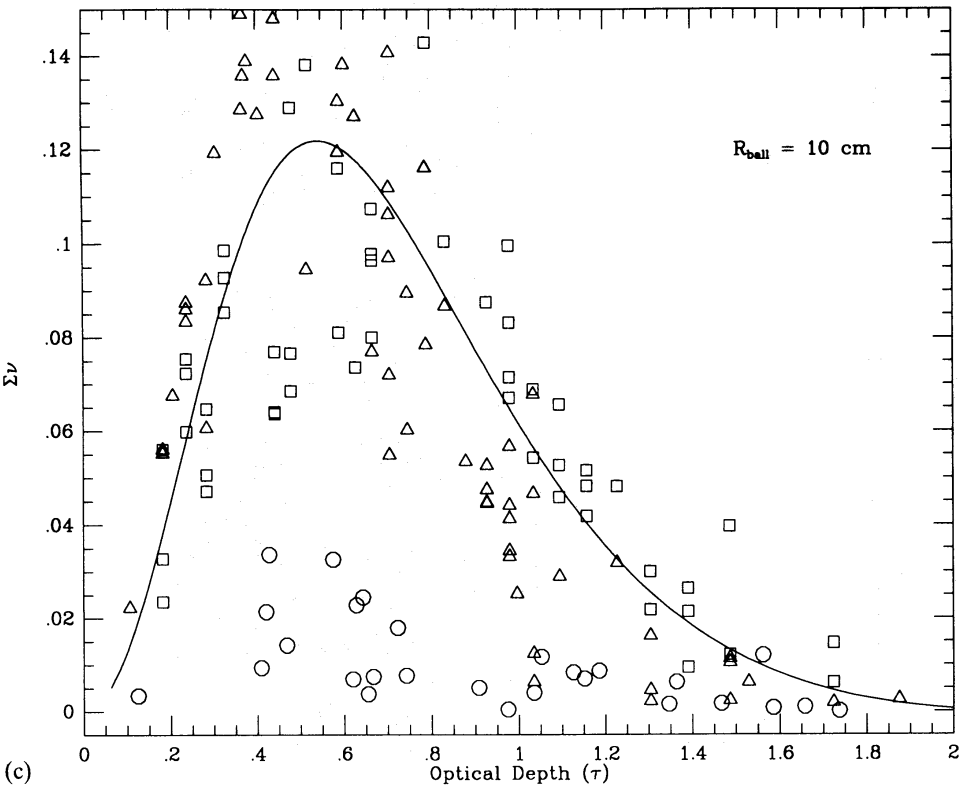

(c)

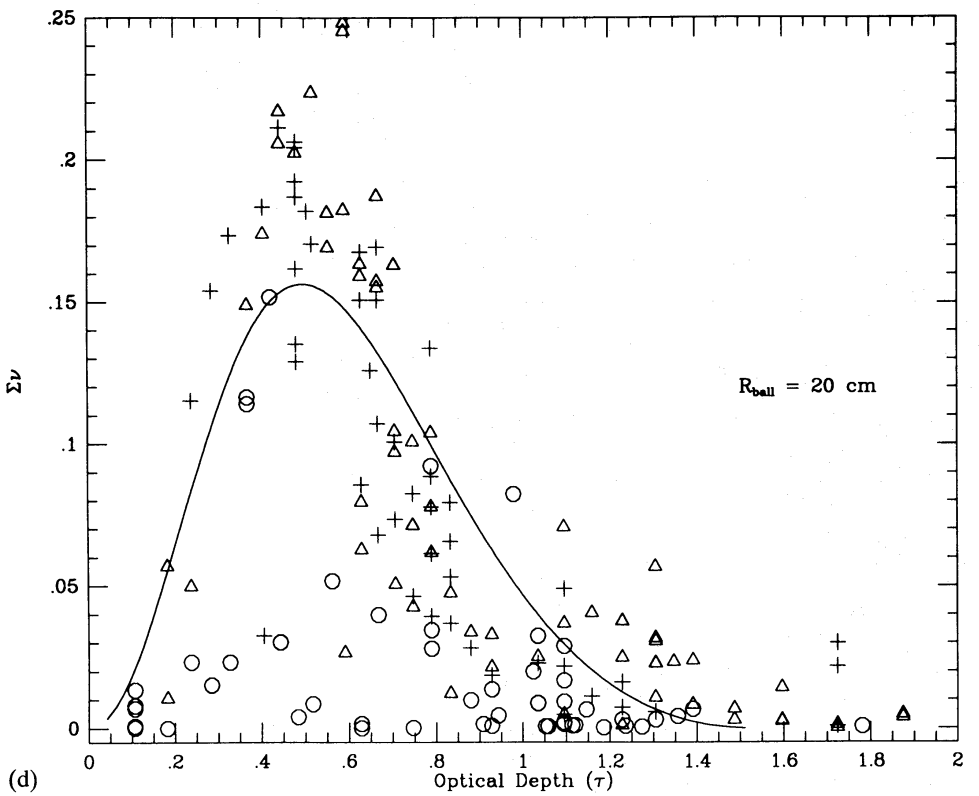

(d)

Figure 15–*continued*

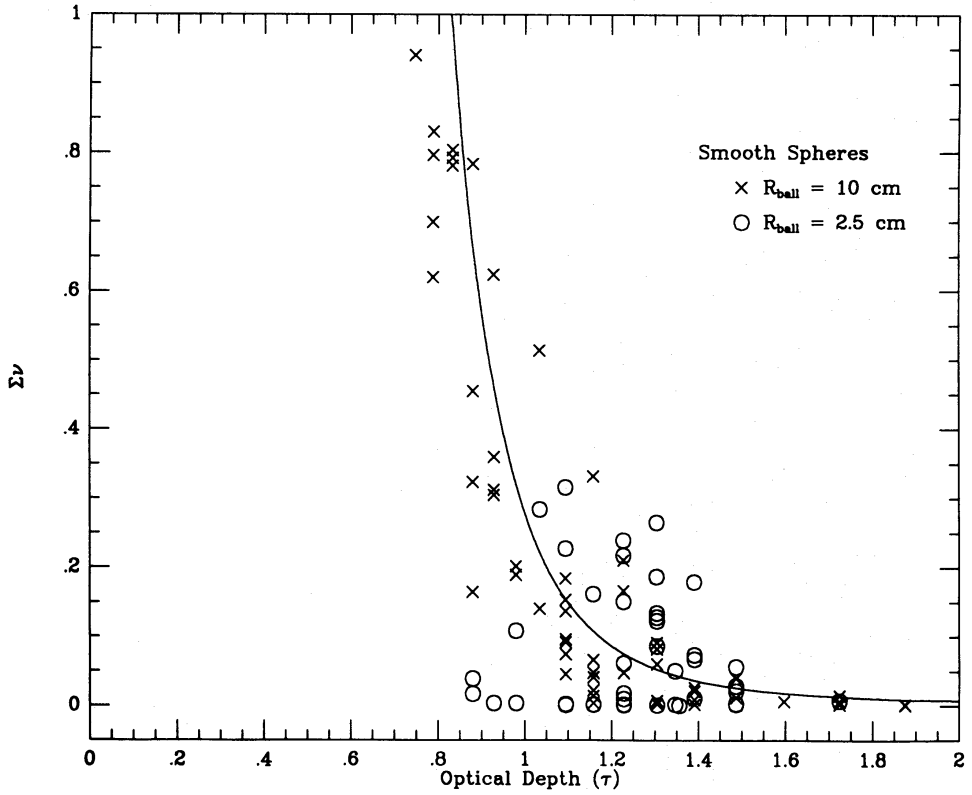

Figure 16. The same as Fig. 15 but for very smooth spheres (Fig. 11).

would imply a wide spread in the relationship between the viscous couple ($\propto \Sigma\nu$) and the surface density Σ. Using the simplest kinematic prescription (Goldreich & Tremaine 1978):

$$(1+\tau^2)(1-\varepsilon^2)\approx 0.6, \tag{2}$$

$$\nu=\frac{v^2\tau}{(1+\tau^2)\,\Omega} \tag{3}$$

where Ω is the orbital angular velocity and ν the kinematic viscosity, we superimpose all our experimental data around an averaged $\Sigma\nu-\Sigma$ relation in Figs 15(a)–(d) and 16. Planetary rings are expected to be viscously unstable in the region where $\Sigma\nu$ decreases with τ.

It has been proposed (Lin & Bodenheimer 1981; Ward 1981; Lukkari 1981) that a viscous instability may be the primary cause for surface density variations in Saturn's B ring. This hypothesis has not been generally accepted because if there is a well defined $\Sigma\nu$–τ relationship, the viscously unstable portion of the ring would probably evolve into discrete ringlets with a bimodal distribution in the surface density (Borderies *et al.* 1984) which is incompatible with observations (Cuzzi *et al.* 1984; Esposito 1986). The results presented in this paper indicate that although there is a general tendency for certain regions of τ to be viscously unstable, there is not a well-defined $\Sigma\nu$–τ relationship. We note that the wide spread in the coefficient of restitution at a given impact velocity implies that the ring system as a whole may be quasi-unstable; some collisions may move the system towards a stable uniform structure, while others may drive the system toward a bimodal distribution, but one in which the position of the ringlets is varying. This might lead to large surface density fluctuations without any indication of a viscous instability driving mechanism.

Finally, we note that, except in the case of very smooth particle surfaces (unrealistic for Saturn's rings), there is a size dependence in the coefficient of restitution. This size dependence

may well be associated with the finite physical extent of the contact region. For particles with a relatively large radius of curvature, minor compression in the contact regions would result in a significant enlargement of the contact area. The elastic deformation during contact is then spread over a large area which reduces the tendency for dislocation and other non-linear dissipative deformation effects. Consequently, collisions between large particles may tend to be more elastic.

It is important to include this dependence in any realistic simulation of planetary rings since the systematic difference in collisional properties between particles with different sizes may cause the particles to segregate according to their sizes. For example, if the relatively large particles encounter elastic collisions with other large particles but dissipative collisions with relatively small particles, their kinematic properties may be quite different from those deduced from analyses which are based on the simplification of the identical particle assumption. Consideration of the size dependence may be particularly relevant in viscously unstable regions of the disc where *Voyager's* data have indeed revealed different spatial density distribution of different sized particles (Marouf *et al.* 1983).

In conclusion, we have presented an extensive set of data on the coefficient of restitution in direct collisions. Some of these data are probably relevant to the dynamics of Saturn's rings. There are of course other complicating factors such as cohesive collisions and grazing or glancing collisions. Data on these important processes will be presented in a later contribution.

Acknowledgments

We would like to thank Bob Carter for machining the disc pendulum and Fritz van Dyke for his aid in the construction of the apparatus as well as for useful comments on the design of various aspects of the experiment. George Hare is deserving of special thanks for his design of the ice ball position detector. We also thank Scott Sachtjen for developing the data acquisition software and for his assistance during many of the experimental runs. We are grateful to NASA for providing funding for this research under grant NAGW590. Lick Observatory Contribution 450.

References

Borderies, N., Goldreich, P. & Tremaine, S., 1984. In: *Planetary Rings,* p. 713, eds Greenberg, R. & Brahic, A., Arizona Press, Tucson, Arizona.

Bridges, F., Hatzes, A. & Lin, D. N. C., 1984. *Nature,* **309,** 333.

Cuzzi, J., Lissauer, J. J., Esposito, L. W., Holberg, J. B., Marouf, E. A., Tyler, G. L. & Boischot, 1984. In: *Planetary Rings,* p. 73, eds Greenberg, R. & Brahic, A., Arizona Press, Tucson, Arizona.

Durisen, R. H., 1984. In: *Planetary Rings,* p. 416, eds, Greenberg, R. & Brahic, A., Arizona Press, Tucson, Arizona.

Esposito, L., 1986. *Icarus,* **67,** 345.

Goldreich, P. & Tremaine, S., 1978. *Icarus,* **34,** 327.

Goldreich, P. & Tremaine, S., 1982. *Ann. Rev. Astr. Astrophys.,* **20,** 249.

Lin, D. N. C. & Bodenheimer, P., 1981. *Astrophys. J.,* **248,** L83.

Lukkari, J., 1981. *Astrophys. Space Sci.,* **61,** 111.

Marouf, E. A., Tyler, G. L., Zebker, H. A. & Eshleman, V. R., 1983. *Icarus,* **54,** 189.

Stewart, G. R., Lin, D. N. C. & Bodenheimer, P., 1984. In: *Planetary Rings,* p. 447, eds, Greenberg, R. & Brahic, A., Arizona Press, Tucson, Arizona.

Shu, F. H., Dones, L., Lissauer, J. J., Yuan, C. & Cuzzi, J. N., 1986. *Astrophys. J.,* **299,** 542.

Whalley, E., 1984. In: *Ices in the Solar System,* p. 9, eds Klinger, J., Benest, B., Dollfus, A. & Smoluchowski, R., Reidel, Dordrecht, Holland.

Ward, W. R., 1981. *Geophys. Res. Lett.,* **8,** 641.